Microscopic Surface and Bulk Morphology of Semicrystalline Poly(dimethylsiloxane)–Polyester Copolymers

A. B. E. Abduallah, P. E. Mallon

Department of Chemistry and Polymer Science, University of Stellenbosch, Matieland 7602, South Africa

Received 26 May 2008; accepted 13 July 2009
DOI 10.1002/app.31103
Published online 7 October 2009 in Wiley InterScience (www.interscience.wiley.com).

ABSTRACT: In this study, two series of semicrystalline poly(dimethylsiloxane) (PDMS)–polyester segmented copolymers with various PDMS contents were synthesized. One series was based on polybutylene adipate (PBA) as the polyester segment and the other was based on a polybutylene cyclohexanedicarboxylate ester (PBCH) segment. The copolymers were characterized using ^{1}H-nuclear magnetic resonance, size exclusion chromatography, dynamic mechanical analyses, differential scanning calorimetry (DSC), and wide-angle X-ray diffraction (WAXD). The microscopic surface morphology and the microscopic bulk morphology were investigated using atomic force microscopy (AFM) and transmission electron microscopy, respectively. The effects of the polyester type and the PDMS content on the crystallinity degree as well as the copolymer surface and bulk morphology at room temperature were investigated for each series. DSC and WAXD results showed the ability of the copolymers to crystallize, to various degrees, depending on the polyester type and the PDMS content. The results showed that the PDMS content had a greater influence on the crystallinity degree in the PDMS-*s*-PBCH (cycloaliphatic) copolymer series than in the PDMS-*s*-PBA (aliphatic) copolymer series. In the copolymers with a low PDMS content, the AFM images showed spherulitic crystal morphology and evidence of PDMS nanodomains in between the crystal lamellae of the ester phase on the copolymer surface. A heterogeneous distribution of the PDMS domains was also observed for these copolymers in the bulk morphology as a result of this segregation between the polyester lamellae. All the copolymers, in both series, showed microphase separation as a result of the incompatibility between the PDMS segment and the polyester segment. Three types of surfaces and bulk morphologies were observed: spherical microdomains of PDMS in a matrix of polyester, bicontinuous double-diamond type morphology, and spherical microdomains of polyester in a matrix of PDMS as the PDMS content increases. J Appl Polym Sci 115: 1518–1533, 2010

Key words: poly(dimethylsiloxane)–polyester copolymer; segmented copolymer morphology; microphase separation; AFM; TEM

INTRODUCTION

The morphology of a multiphase polymer system plays an important role in determining the final properties of the polymers. By controlled variation of the polymer morphology, the desired polymer properties can be obtained. This area of polymer science has attracted wide interest among many researchers who have tried to elucidate the details of microstructure and superstructure using a variety of techniques. The number of investigations dealing with the synthesis and characterization of multiblock copolymers with crystalline and amorphous segments has rapidly increased during the last years.[1–7]

Semicrystalline copolymer morphology has recently received much attention largely because of the ability of these copolymers to exhibit considerable morphological richness.[8–11] This richness of morphology arises from two main factors. The first is the driving force for microphase separation between unlike segments, especially in the melt. This favors the formation of nanoscale domains such as lamellae, spheres, and cylinders. The second factor is the driving force for crystallization of one segment. This favors the formation of alternating amorphous and crystalline layers.[12] When the noncrystallizable segment is glassy during crystallization ($T_g > T_c$), the crystallization occurs within the nanoscale domains as a result of the microphase separation.[12] On the other hand, when the amorphous matrix is soft or rubbery during crystallization ($T_g < T_c$), these two forces compete and, in this case, crystallization often occurs with less morphological constraint. This enables the crystallizable segment to "breakout" and the crystallization overrides any previous melt structure, usually forming lamellar structures and (in many cases) spherulites, depending on

Correspondence to: P. E. Mallon (pemallon@sun.ac.za).

the composition. However, if the strength of the microphase separation is more than the strength of the crystallization, then the crystallization can be only confined to spherical, cylindrical, or lamellar nanoscale domains. This is mainly observed in strongly segregated systems with a rubbery block.[12–15]

poly(dimethylsiloxane) (PDMS)–polyester segmented copolymers are semicrystalline copolymer systems that consist of amorphous–crystalline multiblocks, where the T_g of the PDMS amorphous segment is lower than the T_c of the crystalline polyester segment.[3] These materials can be regarded as thermoplastic elastomers due to the microphase separation of the soft siloxane blocks and the hard polyester blocks. The copolymers demonstrate good mechanical properties, such as impact shock resistance even in low temperature environments, as a result of the low T_g of the PDMS segment. In addition, the films are easily compression molded as a result of the relatively low T_m of the copolymer. Moreover, these materials are expected to be potentially useful in outdoor applications because of their UV stability and the hydrophobicity of the PDMS segment.[1,2] These copolymers have, however, not yet been tested for durability toward ageing and weather effects.

The extremely nonpolar nature of the PDMS structure combined with the weak intermolecular interaction leads to the creation of a polymer phase that is both thermodynamically and mechanically incompatible,[16] not only with the polyester segment but also with virtually all other polymeric systems. This leads to the formation of a multiphase morphology, regardless of whether the other segment is amorphous or semicrystalline. Another important factor to be considered in PDMS copolymers is that the glass transition temperature of the PDMS segment in the copolymer is extremely low. PDMS should behave like a nonpolar viscous liquid at room temperature (at which most characterizations are conducted).[17] Therefore, the low glass transition temperature also provides ideal conditions for the formation of phase-segregated polymer morphologies. The degree of phase segregation between the hard and soft segments depends on their molecular weights and the interaction of the segments with themselves and with each other. Moreover, the interaction between the hard segments depends on the symmetry of the monomer in the polyester segment, and therefore a chain extender having a more symmetrical structure will enhance the formation of organized structures, and thus result in a more complete phase-separated morphology.[18] The morphology of segmented PDMS–polyester copolymers is, therefore, very complicated not only because of their multiphase structure but also because of other physical phenomena, such as crystallization of the polyester segment.

There have been only a small number of studies on the morphology of amorphous–crystalline multiblock copolymers. Most of these studies have been confined to the use of visual inspection by various microscopic techniques. Among the few copolymers that have been studied are the PDMS–polyester segmented copolymers.[3,18] Recently, Miroslawa[3] reported on the spherulitic crystal order of PDMS–polybutyleneterephthalate segmented copolymers. He used thin, quenched cooled films from the melt and investigated the morphology using polarizing optical microscopy (POM). More recently, Childs et al.[18] used atomic force microscopy (AFM) to investigate the surface morphology of polycaprolactone-*b*-polydimethylsiloxane-*b*-polycaprolactone block copolymers. They reported that crystal spherulite structures could be clearly observed using the AFM phase images of the surface. Although the surface morphology of polybutylene adipate (PBA) aliphatic homopolyester has been studied using POM[19] and AFM[20] and recently reported in literature, to date no reports of a systematic investigation of the morphology of PDMS–polyester copolymers with either cycloaliphatic or aliphatic polyester segments have been found. A study of a systematic series of these copolymers will contribute to an understanding of the interrelationship between the phase separation and crystallization of the polyester segments.

The aim of this work is, therefore, to perform a systematic investigation of the surface and the bulk morphology of two series of PDMS–polyester segmented copolymers. In this study, poly(dimethylsiloxane)–polybutylene adipate (PDMS-*s*-PBA) and polydimethylsiloxane–polybutylenecyclohexanedicarboxylate (PDMS-*s*-PBCH) segmented copolymers were selected. This will allow for a study of the effect of an aliphatic and cycloaliphatic polyester segment on the copolymer morphology. Thus, two series of PDMS-*s*-PBA and PDMS-*s*-PBCH copolymers, with a constant PDMS segment length (2000 g/mol) and various PDMS contents, and the homopolymers PBA and PBCH were synthesized via a transesterification reaction under vacuum conditions following the general procedure proposed by Kiefer et al.[2] In this method, the synthetic procedure for obtaining PDMS–polyester copolymers involves the reaction between a diol and diester in the presence of NH_2-terminated polysiloxanes. The latter polymers can be synthesized via the equilibrium ring-opening polymerization of octamethylcyclotetrasiloxane.[7,21]

The obtained copolymers were characterized using ^{1}H-nuclear magnetic resonance (^{1}H-NMR), size exclusion chromatography (SEC), dynamic mechanical analyses (DMA), differential scanning

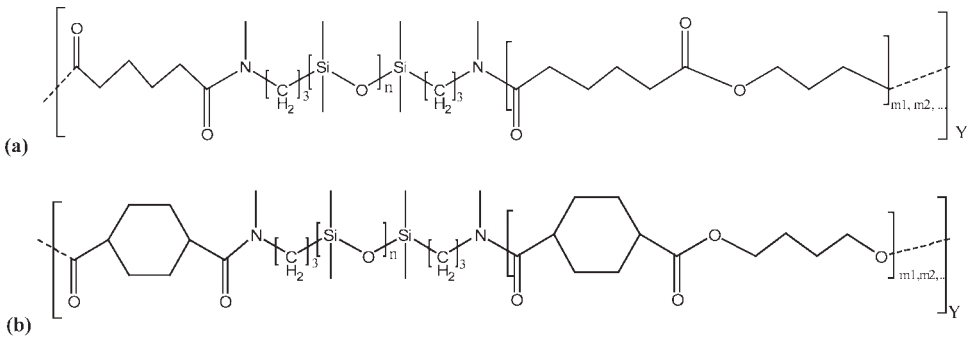

Scheme 1 Chemical structure of poly(dimethylsiloxane)–polyester segmented copolymers: (a) PDMS-*s*-PBA copolymer and (b) PDMS-*s*-PBCH copolymer.

calorimetry (DSC), and wide-angle X-ray diffraction (WAXD) to determine their chemical compositions, molecular masses, glass transition temperatures (T_gs), melting points (T_m), and degrees of crystallinity. The effects of the PDMS content and polyester type on the copolymers surface morphology of thin films as well as the bulk morphology of both copolymer series were investigated using AFM and transmission electron microscopy (TEM), respectively.

EXPERIMENTAL

Materials

1,4-Dimethylcyclohexanedicarboxylate (DMCH, ≥99% purity, 90% cis isomer), adipic acid (AA, ≥99% purity, HPLC), and 1,4-butanediol (BD, 99+% purity) were purchased from Sigma-Aldrich (South Africa) and used without further purification. Titanium tetraisopropoxide (TIP, 99.99% purity) was purchased from Labchem (South Africa), and then it was diluted in freshly distilled toluene to approximately 0.005 g/mL concentration. PDMS with amino functionality and molecular mass of 2000 g/mol was synthesized in our laboratory using the equilibrium ring-opening polymerization for octamethylcyclotetrasiloxane (D_4).[7]

Copolymer synthesis

PDMS-*s*-PBA copolymers [Scheme 1(a)] were synthesized via a condensation reaction between AA, BD, and PDMS. The procedure used to synthesize an alternating block PDMS–polysulfone copolymer was based on the method developed by Auman et al.[22] First, the reactor temperature was increased to melt the AA and BD, and then freshly distilled toluene was added to form a solution of 40% copolymer concentration. After 30 min, 1 mL of the TIP catalyst solution was added to the reaction mixture. The reaction temperature was increased to 140°C under nitrogen gas flow, and after 1 h, the PDMS oligomers were added in the required percentages. The reaction was allowed to continue for 6 h. An additional 0.5 mL of the TIP catalyst was added, and the reaction temperature was raised to 180°C under reduced pressure. The polymerization was continued for 8 h. PBA homopolymer was synthesized in a similar manner.

PDMS-*s*-PBCH copolymers [Scheme 1(b)] were synthesized via a condensation reaction in the melt state between DMCH, BD, and PDMS[2] in two stages. In the first stage, the amino end group of PDMS reacted with DMCH to produce PDMS with an ester end group. In the second stage, DMCH and BD reacted at 170°C under nitrogen flow and in the presence of TIP as catalyst. PDMS with the ester end group was added to the reaction vessel in the required quantity (percentage required). Approximately 6 h after PDMS addition, the excess BD and any remaining methanol were distilled off under high vacuum. The final temperature reached was 220°C. An aliquot of TIP catalyst was added to the reaction mixture prior to drawing vacuum (to achieve high conversions). PBCH homopolymer was synthesized using a similar method.

The synthesized samples were purified from the homopolymers by dissolving the reaction products in chloroform and isolating the copolymers by slow precipitation, using a 1 : 3 mixture of methanol and isopropanol. The copolymers were further purified to remove the remaining PDMS homopolymer by reprecipitation from tetrahydrofuran (THF) into *n*-hexane and then dried at 40°C under vacuum. The purity of the copolymers was confirmed by gradient elution chromatography.

Characterization techniques

The compositions of the resultant PDMS–polyester copolymers were determined from the 300-MHz ^{1}H-NMR spectra, using a Varian Unity Inova instrument. The integrals of the signals assigned to the

methene protons ($\delta = 3.5$ ppm) of the polyester component and the dimethyl protons ($\delta = 0$ ppm) of the PDMS component, after the purified copolymers had been dissolved in chloroform-*d*, were determined.

The average molar mass of the PDMS–polyester copolymers (M_n and M_w) and the polydispersities (M_w/M_n) were determined by SEC using a refractive index (RI) detector. THF was used as an eluent, and the calibration was performed with linear polystyrene standards. Analyses were carried out at 30°C with a system comprising a Waters 610 fluid unit, Waters 410 differential refractometer, Waters 717Plus Auto sampler, and Waters 600E system controller.

Dynamic mechanical analyses (DMA) of the copolymers were carried out on a Perkin Elmer 7e using the thin-film extension mode. Liquid nitrogen was used to cool the samples to −150°C. The frequency was 1 Hz, and the heating rate was 5°C/min. The polymer samples were prepared by casting 10 wt % copolymer solutions in THF solvent on mica substrates. The thickness of the samples was about 0.5 mm.

Differential scanning calorimetric (DSC) analyses of the various copolymers were carried out with a TA Instruments Q100 DSC system. The DSC apparatus was calibrated by measuring the melting temperature of indium metal according to a standard procedure. All measurements were conducted under a nitrogen atmosphere flow and at a purge gas flow rate of 50 mL/min. Polymer samples of 1.0 to 2.0 mg were cooled in aluminum pans from 25 to −30°C at a rate of 10°C/min, held isothermally at −30°C for 5 min, and then heated further at 10°C/min. The melting curve was recorded. The melting temperature (T_m) was determined from the obtained curves, and the area under the crystalline melting peak (ΔH_m) was estimated. The ΔH_m is related to the degree of crystallinity.

WAXD was performed at iThemba LABS (South Africa) on a Bruker AXS D8 ADVANCE diffractometer at room temperature, with filtered Cu Kα radiation, using a LynxEye position sensitive detector. All samples were scanned at diffraction angles (2θ) ranging from 5° to 50°, with a step size of 0.02°. The samples were prepared by casting films of 10 wt % copolymer solutions in THF on mica substrates to form thin films with thickness of about 0.5 mm. From the WAXS data, the percentage of crystallinity was calculated by peak deconvolution and subsequent determination of the relative areas under the amorphous halo and the crystalline peaks of the X-ray diffraction scan. The ratio of the area under the crystalline peaks (I_c) to the total (amorphous + crystalline) area (I_{tot}) gave the degree of crystallinity (ω_m).

AFM images were obtained on a multimode AFM model no. MMAFMLN, with a Nanoscope IIIa controller from Veeco, operating in noncontact mode, and using a low resonance frequency silicon cantilever with a resonance frequency of about 60 kHz and a spring constant of $K = 50$ N/m. The substrate containing the polymer samples was attached to the sample holder with double-sided adhesive tape. All experiments were carried out under ambient conditions. The scan rate was set in the range of 0.5–0.7 Hz. Topography and phase images were captured simultaneously for the tapping mode.

All AFM images were enhanced in the Veeco imaging software program and subjected to a plane fitting and flattening procedure, which eliminates the image bow resulting from nonlinear scanner movement. Additionally, digital filtering was carried out to remove noise and clarify the structures present in the image. Since filtering is a very sensitive process that can generate unreal features or remove existing features, the filtering was kept to a minimum. Only noise and image artifacts were eliminated. The typical sequence of digital filtering applied was autoflattening, planefit, and lowpass filtering. Autoflattening eliminates the image bow by calculating a least square-fitted, second-order polynomial for each scan line, and subtracting it from the scan line. The planefit removes the effect of a skew sample by calculating a best, second-order polynomial planefit and subtracting it from the image. Lowpass filtering is used to remove high frequency noise, such as spikes, by replacing each data point in the image with a weighted average of the points in a 3×3 matrix surrounding the point.

AFM samples were prepared as ultrathin films by the solution casting method on mica wafers (1×1 cm^2). One drop of 0.5 wt % copolymer in THF was placed on the mica plate and then covered with another mica plate to spread the solution between the two mica plates. The two mica plates were slid against each other in opposite directions to form an ultrathin film of 10 to 5 μm. The films were dried at room temperature for 24 h.

TEM experiments were performed on the ultrathin films of PDMS–polyester copolymers using a JEOL 200 CX instrument (University of Cape Town). The copolymers films were prepared, using a solvent casting technique, from 10 wt % copolymer in THF, followed by cryo-ultra-microtoming of very thin slices, with a thickness of about 40–60 nm, cut at −100°C.

RESULTS AND DISCUSSION

Copolymer characterization

The chemical compositions and molar masses of the PBA and PBCH copolymer series are shown in Table I. Experimental values of the PDMS contents

TABLE I
The Chemical Compositions and the Average Molecular Weights of PBA and PBCH Homopolymers, and PDMS-*s*-PBA and PDMS-*s*-PBCH Copolymers, Prepared Using Different PDMS Concentrations

Sample no.	PDMS in feed (wt %)	PDMS in the copolymer[a] (wt %)	PDMS unreacted (ratio to PDMS in the feed)	Extracted materials[b] (wt %)	M_w[c] (g/mol)	M_n[c] (g/mol)	M_w/M_n
PBA	0	0.00	–	–	15,795	8143	1.94
A-1	5	4.57	0.082	12.84	11,239	6314	1.78
A-2	10	8.97	0.103	11.27	17,700	9415	1.88
A-3	25	21.70	0.132	12.22	18,066	9819	1.84
A-4	40	34.20	0.147	16.44	14,310	8131	1.66
A-5	60	51.10	0.149	18.81	12,568	7141	1.76
PBCH	0	0.00	–	–	27,719	17171	1.66
B-1	5	4.74	0.052	7.20	25,990	16665	1.76
B-2	10	9.20	0.080	6.35	27,719	17171	1.62
B-3	25	22.70	0.092	7.38	34,502	20239	1.71
B-4	40	35.76	0.107	8.75	32,720	18568	1.70
B-5	60	52.10	0.132	11.34	31,204	16860	1.85

[a] Measured by ^{1}H-NMR.
[b] Calculated as weight percent using the weight of the product after extraction compared with the weight before extraction.
[c] Measured by SEC.

(wt %) in the copolymers were determined from the ^{1}H-NMR spectra. These are shown in Table I. It is clear that the experimental values of the PDMS content were somewhat lower than the theoretical values determined from the feed in the copolymerization reactions. The quantity (weight ratio of the unreacted PDMS to the PDMS in the feed) of unreacted PDMS increases with an increase in the PDMS content for both types of the PDMS–polyester copolymers. The lower polarity of the PBCH monomers (DMCH), when compared with the PBA monomers (AA), results in better compatibility or miscibility of the PBCH with the nonpolar PDMS oligomers in the copolymerization reaction, and thus the percentages of unreacted PDMS for the aliphatic polyester (PBA) are higher for the cycloaliphatic polyester (PBCH) series. Both copolymers series did, however, show greater PDMS incorporation with a higher PDMS feed ratio.

SEC results (Table I) show that the number-average molecular weights of PDMS–polyester copolymers ranged from about 20,239 to 16,665 g/mol for PDMS-*s*-PBCH series, and the maximum M_n for PDMS-*s*-PBA was 9819 g/mol. There is, however, no clear effect or change in the M_n of the copolymers with the change in the PDMS content. In the case of very low content PDMS copolymer, there is a possibility as some chains do not contain any PDMS segment. The polydispersity values over the entire series were less than two. This demonstrates the high efficiency of extraction of the small species of either homopolymers or copolymers during the purification step. The weight percentages of the materials extracted during the purification step are tabulated in Table I. The total weight percentages of the extracted material are between 11.27 and 18.81 wt % for the PDMS–PBA copolymer series and between 6.35 and 11.34 wt % for the PDMS–PBCH copolymer series.

Multicomponent PDMS–polyester copolymers are expected to show a multiphase structure of a soft amorphous phase of PDMS and a relatively less soft phase of polyester, in addition to the polyester crystalline hard phase. DMA was used to determine the T_g values of both amorphous phases. Table II shows the T_g values of the PDMS–polyester copolymers with various PDMS contents. Two glass transition temperatures were observed for all the copolymers in the series of the segmented copolymers. The fact that the T_g values of the PBA and PBCH homopolymers are -50°C[23] and 15°C,[2] respectively, and the T_g value of the PDMS homopolymer is -123°C[17] suggests that the higher T_g in the copolymer is due to the polyester segment and the lower T_g is due to the PDMS segment. In the PDMS-*s*-PBCH series, a secondary transition was observed at about -50°C. This was very clear for copolymers with a low PDMS content. The secondary transition was also observed for the PBCH homopolymers. This transition is related to the polyester segment, as reported by Kiefer et al.[2] The presence of two T_g values implies a segregated morphology on the micro or nanoscale. The low T_g values of the PDMS–polyester copolymers (except for A-1 and B-1, Table II) remained more or less constant. The independence of the T_g values indicated that the PDMS–polyester copolymers exhibited a high degree of phase separation. The nature of the phase-separated morphology was further investigated using TEM and AFM.

TABLE II
Glass Transition Temperature (T_g), Melting Temperature (T_m), and the Degree of Crystallinity of PBA and PBCH Hompolymers, and PDMS-*s*-PBA and PDMS-*s*-PBCH Copolymers, with Various Polyester Contents

Sample no.	Polyester (wt %)	T_gL[a] (°C)	T_gH[b] (°C)	T_m (°C)	ΔH_m (J/g)	$\Delta H_{m\mathrm{PES}}$ (J/g)	Crystallinity ω_m[c] (%)	Crystallinity $\omega_{m\mathrm{PES}}$ (%)
PBA	100.00	–	−66	58.1	53.4	53.4	43.6	43.6
A-1	95.43	–	−68	57.7	50.4	52.8	39.5	41.4
A-2	91.03	−118	−73	56.7	43.2	47.5	35.8	39.3
A-3	78.30	−119	−73	55.9	21.9	27.9	30.9	39.5
A-4	65.80	−123	−79	54.7	18.8	28.6	23.9	36.3
A-5	48.90	−123	−82	54.2	4.5	9.2	16.2	33.1
PBCH	100.00	–	15	67.7	79.1	79.1	31.4	31.4
B-1	95.26	−94	12	62.2	42.3	44.4	23.4	24.6
B-2	90.80	−115	5	61.1	28.4	31.3	16.4	18.0
B-3	77.30	−118	−5	60.9	15.1	19.5	14.1	18.2
B-4	64.24	−123	−3	57.2	12.2	18.9	9.61	14.9
B-5	47.90	−121	−7	55.7	1.5	3.1	6.10	12.7

[a] The lowest glass transition temperature measured from tan δ curve.
[b] The highest glass transition temperature measured from tan δ curve.
[c] The degree of crystallinity measured from WAXD data.

Table II shows the results of the DSC analyses of both copolymer series. Analyses were carried out to investigate the effect of the PDMS content on the melting temperature and the degree of crystallinity in the samples. The degree of crystallinity is related to the enthalpy of melting (ΔH_m), which is determined from the area under the melt peak in the DSC thermogram. Table II shows that the polymer crystallinity decreases with an increase in the weight fraction of PDMS in the copolymer. Similar results were obtained for the melting point. The enthalpy of melting based on the polyester content ($\Delta H_{m\mathrm{PES}}$) was calculated using the weight fraction of the polyester in the copolymers and the enthalpies of melting (ΔH_m). The results obtained are shown in Table II. It is clear that for both series of copolymers the crystallizability of the polyester decreased as the PDMS content increased. WAXD analysis was also used to obtain the actual crystallinity degree and more information about the changes in the copolymer crystal regions and in the crystallinity types. These results are illustrated in Figure 1 and summarized in Table II.

Figure 1 shows the WAXD spectra for the PDMS and homopolymers of the polyesters as well as for the PDMS-*s*-PBA and PDMS-*s*-PBCH copolymer series. Copolymer samples with a PDMS content of more than 10% showed a characteristic amorphous halo (small shoulder) at $2\theta = 12.5°$. This is related to the PDMS amorphous region. It is clearly observed for the PDMS homopolymer in Figure 1(b) and the insert in Figure 1(a). The position of this halo does not change in the copolymers, confirming the formation of relatively pure PDMS microdomains. This phenomenon has been reported for other PDMS copolymers such as PDMS–polyurethane segmented copolymers.[24]

Figure 1(a) indicates that the WAXD spectrum for the PBA and PDMS-*s*-PBA copolymers have very sharp peaks at 21.8°, 24.5°, and 30.3°. On the other hand, sharp peaks were not observed in Figure 1(b) for the PBCH and PDMS-*s*-PBCH copolymers at 15.3°, 18.2°, 20.5°, 22.1°, and 28.6°. The fact that the same peaks were observed within each series indicates that the polyester segments have more or less the same crystalline structure in the homopolymers as that in the respective copolymers. The decrease in intensity of crystallinity peaks as the PDMS content increases indicates that the total degree of crystallinity decreases for the copolymers. The percentage crystallinity (ω_m) was calculated by peak deconvolution, and the subsequent ratio of the area under the crystalline peaks (I_c) to the total (amorphous + crystalline) area (I_{tot}) gave the degree of crystallinity (ω_m), according to the following equation:

$$\omega_m(\%) = (I_c/I_{\mathrm{tot}}) \times 100 \quad (1)$$

Results of calculations from the wide-angle X-ray data of the thin films are tabulated in Table II. There was a significant reduction in crystallinity of the copolymers as the PDMS content increased in both copolymer series similar to that observed in the DSC data. The degree of the crystallinity based on the polyester content ($\omega_{m\mathrm{PES}}$) was calculated using the degree of crystallinity (ω_m) and the polyester weight fraction. The obtained values are tabulated in Table II. It is clear from the $\omega_{m\mathrm{PES}}$ values that there was a decrease in crystallinity of the polyester segments from 43.60% for PBA to 33.12% for the A-5 copolymer and from 31.40% for PBCH to 12.73% for the B-5 copolymer. In all cases for the copolymers with similar PDMS contents, the PDMS-*s*-PBCH copolymer series showed a greater decrease in polyester

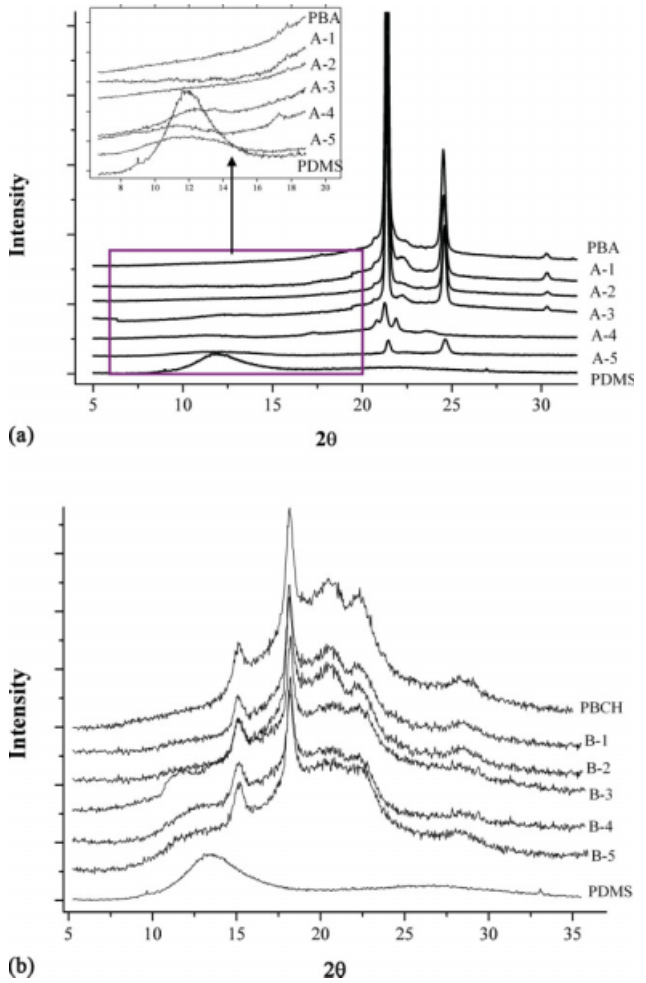

Figure 1 WAXD profiles of (a) PDMS and PBA homopolymers and PDMS-*s*-PBA copolymers with various PDMS contents, including magnification of the region from 2θ = 6° to 18°, and (b) PDMS and PBCH homopolymers and PDMS-*s*-PBCH copolymers with various PDMS contents. [Color figure can be viewed in the online issue, which is available at www.interscience.wiley.com.]

crystallinity degree relative to the PDMS-*s*-PBA copolymer series. The PDMS content, therefore, has a greater influence on the polyester crystallinity in the cycloaliphatic series relative to the aliphatic series. This may be attributed to one of the following reasons or a combination of both. First, the low T_g (–66°C) of the PBA segment allows more PBA segments to arrange in the crystalline phase than the higher T_g PBCH segment (15°C). This large difference in chain mobility can result in decreased PBCH segment crystallinity. Second, the large difference in polarity (calculated using Small's method[25]) between the PDMS segment [7.34 $(cal/cm)^{1/2}$] and the PBA segment [8.84 $(cal/cm)^{1/2}$], when compared with the PBCH segment [7.94 $(cal/cm)^{1/2}$], during the copolymerization, could lead to a broader PBCH segment distribution in the copolymer chains and therefore a higher degree of mixing in the PDMS-*s*-PBCH copolymer series than that in the PDMS-*s*-PBA copolymer series.

Microscopic surface morphology of the copolymers

The surfaces of thin films of the homopolymers and the segmented copolymers (prepared by the casting method) were imaged via tapping mode AFM at ambient temperature. The resulting topography or height images and phase images are shown in Figures 2–4 and 6 and 7. For the sake of the simplicity of discussion, the starting PDMS content is used in the text; the actual copolymer content is given in Table I. Figure 2 shows the topography (left images) and phase images (right images) for the PBA (a,b) and PBCH (c,d) homopolymers. Both polymers show clear semicrystalline spherulitic morphology. Although it is possible to distinguish the spherulitic structures from the height images of the AFM, it is clear that the phase images provide more detailed information about the spherulitic crystal structure than the height images. This is especially true in the case of the PBCH homopolymer. The height images obtained using the tapping mode are not 100% reliable for copolymers with different segments or blocks because the relative contrast of the different blocks depends sensitively on the driving frequency in the height images, which does not exist in the phase images.[26,27] However, the information obtained from the phase images complements the information obtained from the height images. Most of our discussion will therefore focus on the phase images. Similar types of spherulitic crystal structure observed in this study for the PBA homopolymer has been reported by Frömsdorf et al.[20]

The surface morphologies of the PDMS-*s*-PBA and PDMS-*s*-PBCH copolymers with a 5% PDMS content are shown in Figure 3. The AFM phase images show well-defined spherulitic crystal morphology for both the PDMS-*s*-PBA (A-1) and the PDMS-*s*-PBCH (B-1) copolymers. These spherulites seem to grow from primary nuclei and then develop as globular aggregates for both of the copolymers. The size of the spherulites is relatively large, that is, the diameters of the spherulites for both copolymers are in the range 20–30 μm. This variation in the spherulites size (or diameter) and the particular curvature of the frontier between neighboring spherulites indicates that the spherulites are not simultaneously nucleated.[28] The appearance of the spherulitic crystal structure for these copolymers is probably due to a small PDMS content, which obviously leads to longer polyester segments in the copolymers and allows the chain to fold, forming a lamella crystal structure. A similar type of morphology to that observed for PDMS–polyester copolymers in this study has been

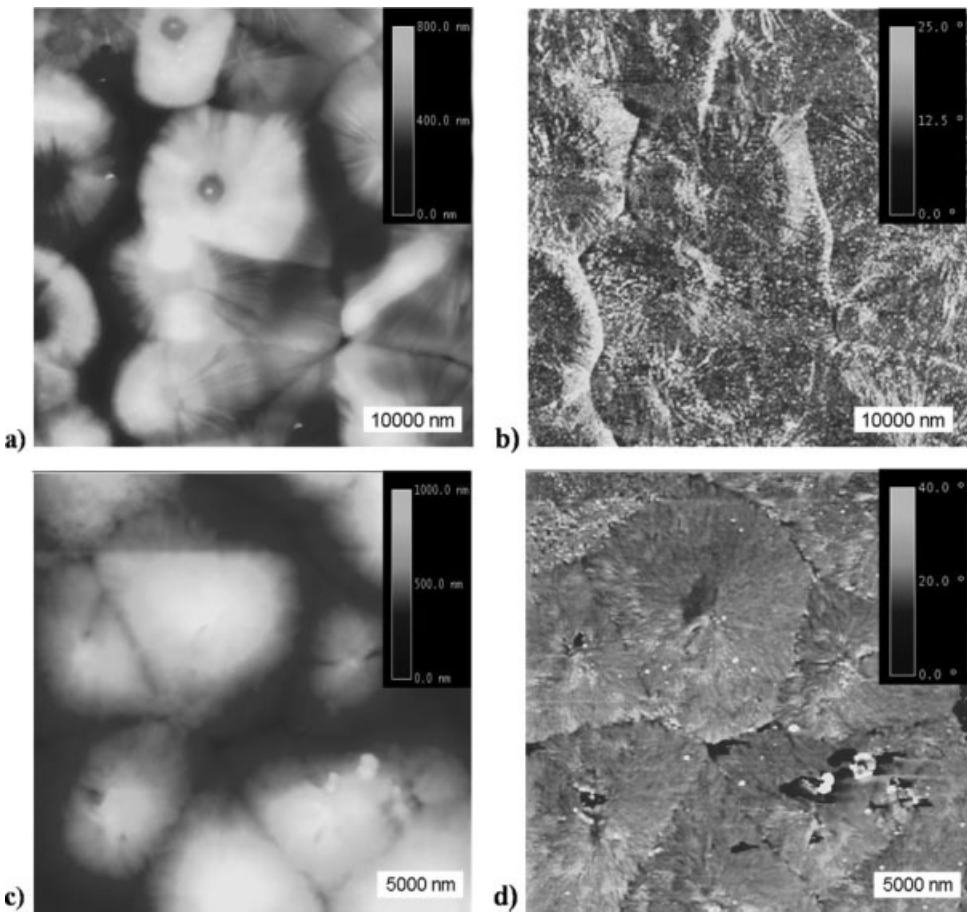

Figure 2 Topography and AFM phase images of thin films of polyester homopolymers: (a and b) aliphatic polyester (PBA) and (c and d) cycloaliphatic polyester (PBCH).

reported by Miroslawa for PDMS–polybutylene terephthalate segmented copolymers using POM.[3]

Figure 4 shows the AFM phase images obtained for the homopolymer and the copolymer surfaces using a high AFM resolution or higher magnification. This figure shows that the spherulites comprise close-packed lamellae. By comparing the lamellae arrangement and thickness for PBA and PBCH [Fig. 4(a) and (c), respectively], one can see that PBCH has a larger lamella thickness than PBA. This difference in the lamella thickness is believed to be kinetically selected as a result of the differences between the PBA and the PBCH polyesters in terms of the crystallization rate, state of entanglement, molecular weights, and the interfacial energy. In the case of the PDMS-*s*-PBA and PDMS-*s*-PBCH copolymers, small spherical domains were detected in between the lamellae inside the spherulitic crystal structure, as shown in Figure 4(b,d). The average size or diameter of these domains is approximately 25 ± 5 nm for PDMS-*s*-PBA copolymers and 30 ± 5 nm for PDMS-*s*-PBCH copolymers. On the other hand, in Figure 4(a,c) no domains are seen for PBA and PBCH homopolymers. Therefore, it is believed that these domains in the copolymer are PDMS segments segregated to form PDMS domains or islands (dark spots in the phase images) in the polyester matrix (the bright region in the phase images). In literature, two different theories have been suggested to interpret phase images in terms of sample properties. The first[29–32] relates the contrast of the phase images to surface stiffness, and the second[33–35] relates the contrast of the phase images to the energy dissipation at the AFM tip and the sample surface interface. However, both of these theories agree that different components in a heterogeneous material or system, such as PDMS–polyester copolymer systems, can be distinguished from the phase images. PDMS and polyester are different both chemically and mechanically, and a combination of both these differences leads to variations between the PDMS regions and polyester regions in terms of the elasticity or viscoelasticity properties, as well as in the energy dissipation between the sample surface and the AFM tip interface.

Figure 5 is a schematic illustration demonstrating how the PDMS domains form between the lamella structures in the PDMS–polyester copolymers. The

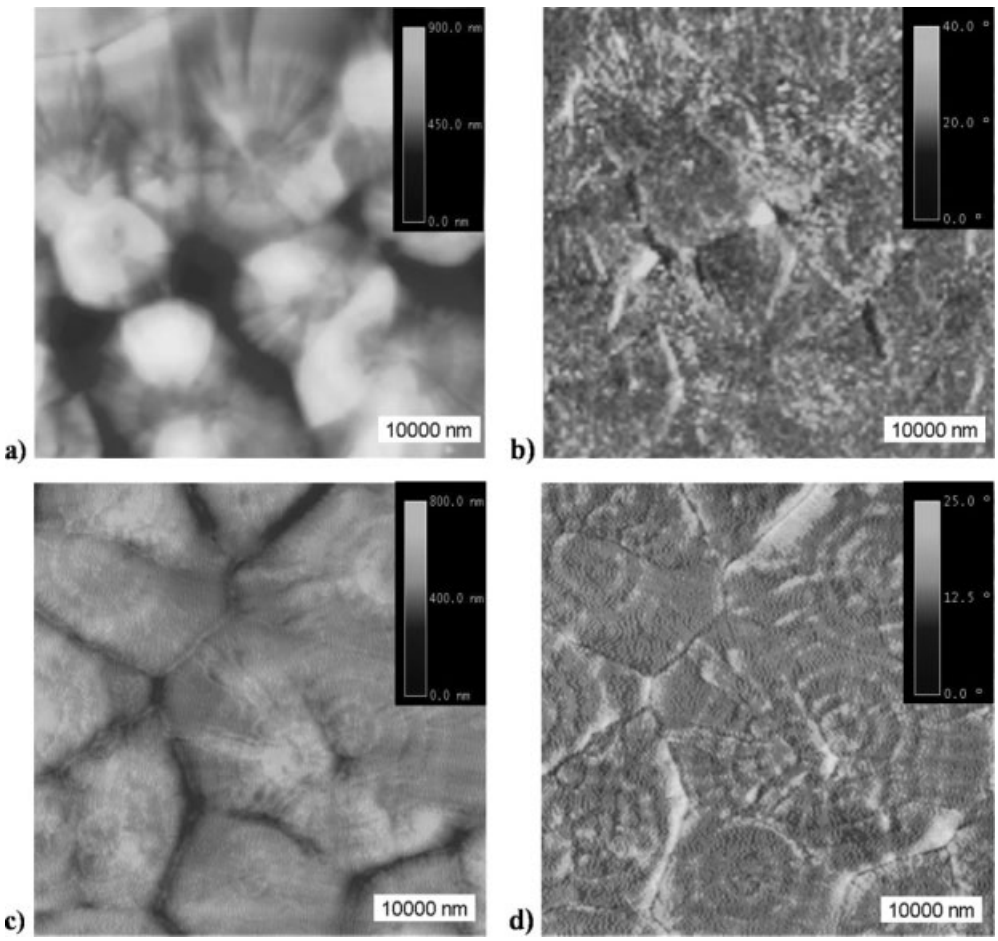

Figure 3 Topography and AFM phase images of thin films of poly(dimethylsiloxane)–polyester copolymers with 5% PDMS (M_n PDMS segment 2000): (a and b) PDMS-*s*-PBA and (c and d) PDMS-*s*-PBCH.

fact that spherulites as well as small amounts of spherical domains were observed in these copolymers suggests that liquid–liquid demixing had occurred, where the major part of the phase-separated PDMS segments seem to be present as spheres in between the crystalline phases of the polyester.

Figure 6 shows AFM images of the 10% PDMS–polyester copolymers. A slightly different morphology to the 5% PDMS content copolymer morphology was observed for these higher content copolymers (A-2 and B-2). First, in the case of the PDMS-*s*-PBA copolymers [Fig. 6(a)], the dominant type of surface morphology is a spherulitic crystal structure. Once again, spheres of PDMS domains appear in the phase images. However, the PDMS domains appear larger and concentrated around (or more noticeable around) the boundaries of the spherulites. In the case of the 10% PDMS-*s*-PBCH copolymer [Fig. 6(b)], spheres of the PDMS domains are also observed in the AFM phase images, but no spherulitic crystal structures are observed, even in AFM images of smaller magnification (larger images size 50 μm × 50 μm). In this case, the diameters of the PDMS spheres are greater than 50 nm, which is about twice as large as the diameter measured for the 5% PDMS in PDMS-*s*-PBCH copolymer series. This might be due to the increase in PDMS content, which leads to shorter polyester segments and the incorporation of more PDMS segments in the copolymer chain. There is also a possibility that a very small percentage of short polyester segments may be trapped inside the PDMS domains. The absence of an observable crystal structure on the surface of the PDMS-*s*-PBCH copolymer is also reflected by the dramatic decrease (13.34% decrease) in the polyester crystallinity ($\omega_{m\mathrm{PES}}$) in the copolymer relative to that for the PDMS-*s*-PBA copolymer with 10% PDMS content (4.28% decrease).

When the PDMS content increases to 25%, no spherulites are detected by AFM on the surface for either type of copolymer. This is most probably due to the presence of relatively smaller amounts of crystallinity in these copolymers, as detected by DSC and WAXD, and the decreased probability of the formation of crystals at the interface. The PDMS domains on the surface increase in number as well as in size. The average diameter of the PDMS

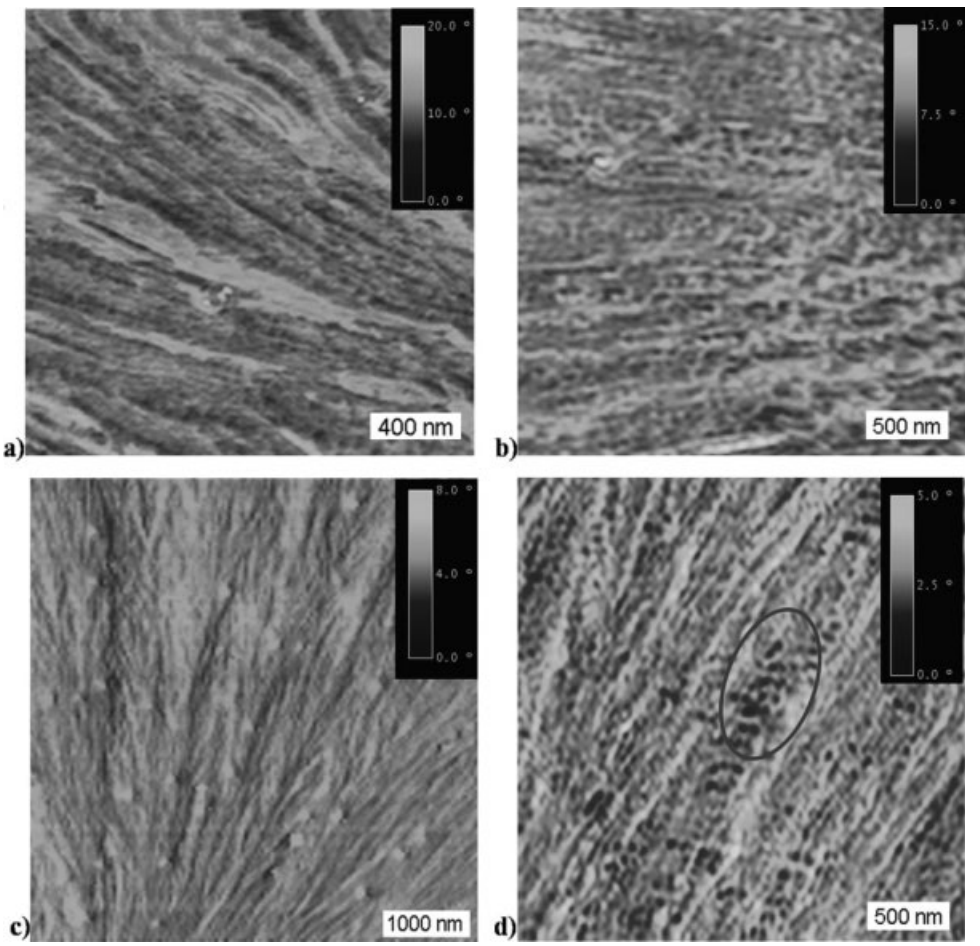

Figure 4 AFM phase images of higher resolution of thin films of polyester homopolymers and poly(dimethylsiloxane)–polyester copolymers with 5% PDMS: (a) PBA, (b) PDMS-*s*-PBA copoylmer, (c) PBCH, and (d) PDMS-*s*-PBCH copolymer.

domains in the PDMS-*s*-PBA copolymers (A-3) [Fig. 7(a)] is more than 70 nm, and in the PDMS-*s*-PBCH copolymers (B-3) [Fig. 7(b)] it is more than 60 nm. The standard deviation increases to 10 nm. As the concentration of the PDMS increases to 40% (A-4 and B-4) [Fig. 7(c,d)], the spherical PDMS domains start connecting with each other and a bicontinuous double-diamond type of morphology appears on the surface. Upon a further increase in PDMS content to 60% (A-5 and B-5) [Fig. 7(e,f)], this type of morphology changes to spheres of polyester surrounded by rubbery phases of PDMS.

The results of the WAXD, DSC, and AFM analyses show that the crystallization of the polyester segments in the PDMS–polyester copolymers is commonly affected by the PDMS component. A high PDMS content has a stronger inhibition effect on the crystallization of the polyester component for the PDMS-*s*-PBCH copolymer series than for the PDMS-*s*-PBA copolymer series. The inhibition of the crystallization of the polyester segment makes the observation of the crystallization at the surface increasingly difficult upon increasing PDMS content. This, combined with the strong preferential surface segregation of the PDMS components, means that no crystal morphology is observed via AFM in the higher content PDMS copolymers (above 10% PDMS content). In the case of the cycloaliphatic series, no crystal morphology was observed for copolymers above a 5% PDMS content due to the greater inhibition of crystallization by the PDMS in this series.

The high-content PDMS copolymers showed spherical domains of the PDMS phase embedded in a matrix of polyester phase. This type of morphology changed from spherical domains to bicontinuous double diamond to a PDMS dominant phase. Unlike the lower content PDMS copolymers, there was no indication of PDMS domains between the crystal structure, and any crystallinity in the high-content PDMS copolymers was confined within the spherical microdomains of the polyester that are prescribed by microphase separation. A similar observation was reported for other block copolymers such as poly(ethylene)-*b*-poly(styrene-*r*-ethylene-*r*-butene) by Loo et al.[36]

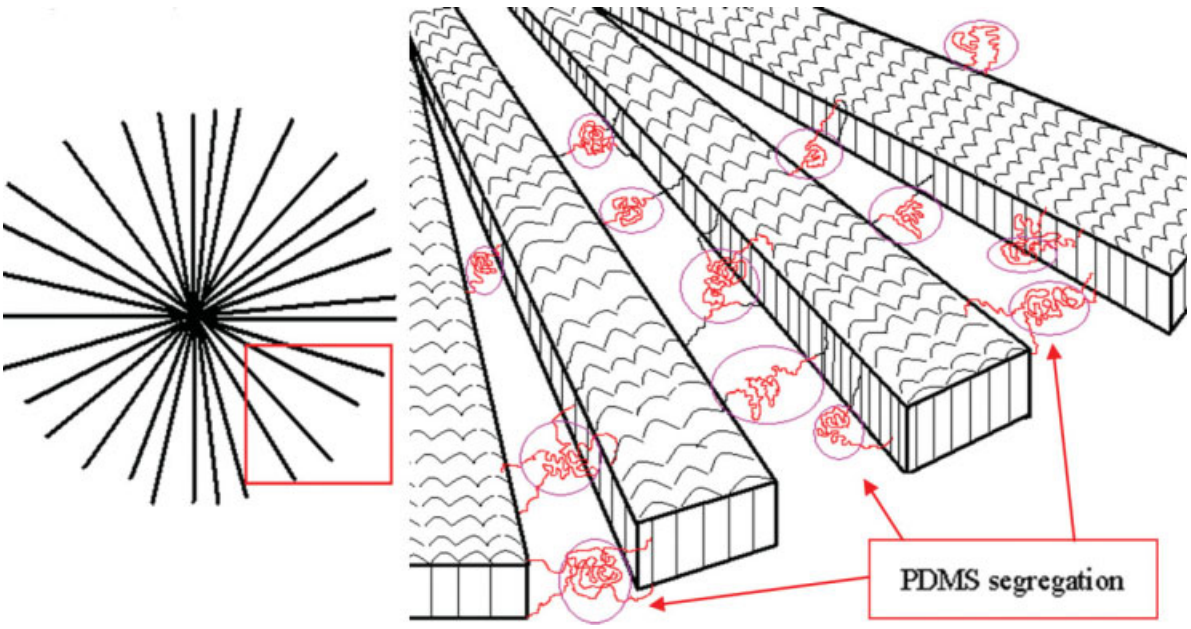

Figure 5 Schematic illustration of the PDMS segregations in between the lamellae arrangements in the poly(dimethylsiloxane)–polyester copolymers. [Color figure can be viewed in the online issue, which is available at www.interscience.wiley.com.]

Microscopic bulk morphology of the copolymers

TEM images, illustrated in Figures 8 and 9, clearly show that all the PDMS–polyester copolymers had distinct microphase separation. This supports the results of the T_g measurements that were obtained by DMA. Figure 8 shows TEM micrographs of a cross-section of the PDMS-*s*-PBA and PDMS-*s*-PBCH copolymers with various PDMS contents. One can distinguish dark areas, which are related to the PDMS phase due to its higher electron density relative to the polyester. Thus, the polyester homopolymer is essentially featureless. At 5% PDMS content [Fig. 8(a,b)], very fine microphase domains in spherical shapes are observed for both types of copolymers. These spheres are believed to be due to the segregation of PDMS segments. A similar type of morphology was detected for the 10% PDMS content copolymers [Fig. 8(c,d)]. The TEM micrograph of a 5% PDMS content copolymer suggests that the submicron domains do not seem to be homogenously distributed [see the oval in Fig. 8(a,b)] when compared with the TEM micrograph of a 10% PDMS content segmented copolymer. In the case of the 5% PDMS content copolymers, this could be as a result of the PDMS segregating between or around the lamella crystal structure, as shown for the PDMS-*s*-PBA and PDMS-*s*-PBCH copolymers, of thin film surfaces in Figure 4(b,d). In contrast to the 5% PDMS content copolymers, the PDMS domains in the 10% PDMS content copolymers appear to be more evenly distributed in the polyester matrix. This is due to the lower degree of crystallinity in these copolymers when compared with the 5% PDMS content copolymers. Similar results of microdomain phase separation have been reported by Van der Schuur et al.[37] for poly(propyleneoxide) based polyether(ester-amide)s with noncrystallizable amide segments.

The bulk morphology of the PDMS-*s*-PBA copolymer series was similar to the PDMS-*s*-PBCH copolymer series as shown by TEM. However, the average size of the PDMS domains of copolymer A-1 [Fig. 8(a)] is 10 ± 3 nm, which is smaller than that of B-1 [approximately 25 ± 5 nm, Fig. 8(b)]. This could be because less PDMS was incorporated into A-1 copolymer, and hence fewer PDMS segments segregated with each other, forming smaller spherical PDMS domains (when compared with the B-1 copolymer). On the other hand, in the case of A-2 copolymer [Fig. 8(c)], the average diameter of the PDMS domains was 200 ± 50 nm. This value is much larger than that of B-2 copolymers [40 ± 10 nm, Fig. 8(d)], even though the actual PDMS content for A-2 copolymer (8.97 wt %) was less than that for B-2 copolymer (9.20 wt %). This suggests that decreasing the polarity of the polyester phase (an aliphatic polyester has higher polarity than a cycloaliphatic polyester) favors the more discrete microdomain structure (PDMS segregations), with a higher surface-to-volume ratio.

The average diameter of the nanospherical domain of the 5% PDMS content copolymers, as measured from the TEM images, is smaller than that measured

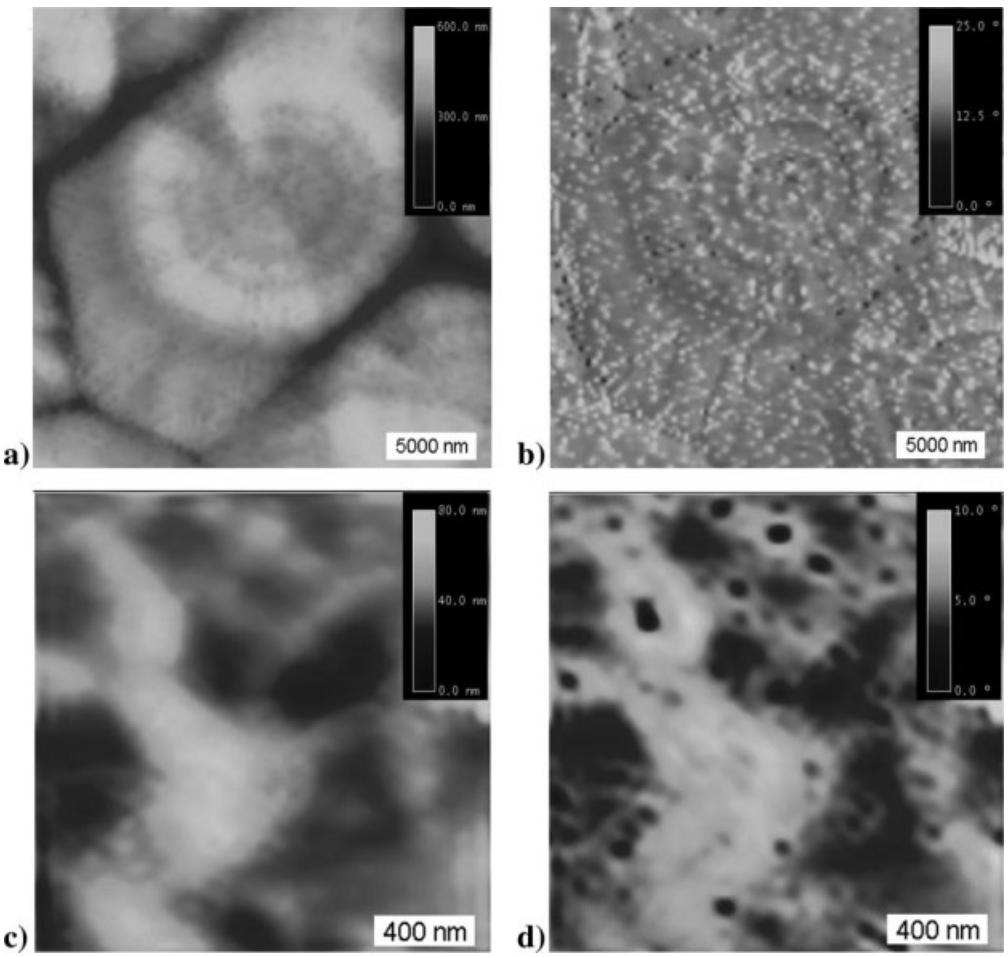

Figure 6 Topography and AFM phase images of thin films of poly(dimethylsiloxane)–polyester copolymers with 10% PDMS (M_n PDMS segment 2000): (a and b) PDMS-*s*-PBA and (c and d) PDMS-*s*-PBCH.

from AFM images on the thin film surface. This may be due to one or all of the following three reasons. First, when measuring very small objects using the AFM, the actual size of the AFM tip cannot be neglected; the measured profile is in fact a convolution of the actual profile and the tip shape. However, correction procedures have been developed that can be applied.[38] Second, flattening can occur,[39] especially when the surface consists of soft material such as PDMS segments. This problem can be minimized by using the tapping mode of AFM. The third reason arises from the affinity of the PDMS segments to diffuse to the copolymer surface.[40] The PDMS at the surface is expected to have a substantially higher concentration than its overall bulk concentration, which might lead to the formation of larger microdomains of the PDMS on the surface than in the bulk.

The difference in the samples preparation conditions for the AFM and TEM analyses was expected to lead to significantly different bulk and surface morphologies, where samples of higher polymer concentrations were used for TEM analysis. In addition, the PDMS component will segregate on the copolymer surface. This has been reported for various copolymers with one PDMS segment or block.[41,42] Surprisingly, there was a high degree of similarity in the type of morphology of the copolymers determined by AFM and TEM. This might be a result of using very thin films for the copolymers in the surface analyses.

As the PDMS content in the PDMS-*s*-PBA and PDMS-*s*-PBCH copolymers increased, a different bulk morphology started to form: in the 25% PDMS content copolymers, the PDMS spheres started connecting to each other [Fig. 9(a,b)]. This indicates that the copolymer morphology or the type of microphase separation is dependent on the PDMS content. This is clearly seen when the spheres completely disappear in the 40% PDMS content copolymers and the morphology changes to bicontinuous or co-continuous phases, as seen in Figure 9(c,d). In this micrograph, the PDMS phase and polyester phase are both represented as being continuous and interpenetrating. This requires a sufficient amount of hard segments (about 60% polyester). Any crystallinity in the copolymer would be limited to the polyester domains. In the 60% PDMS content copolymers

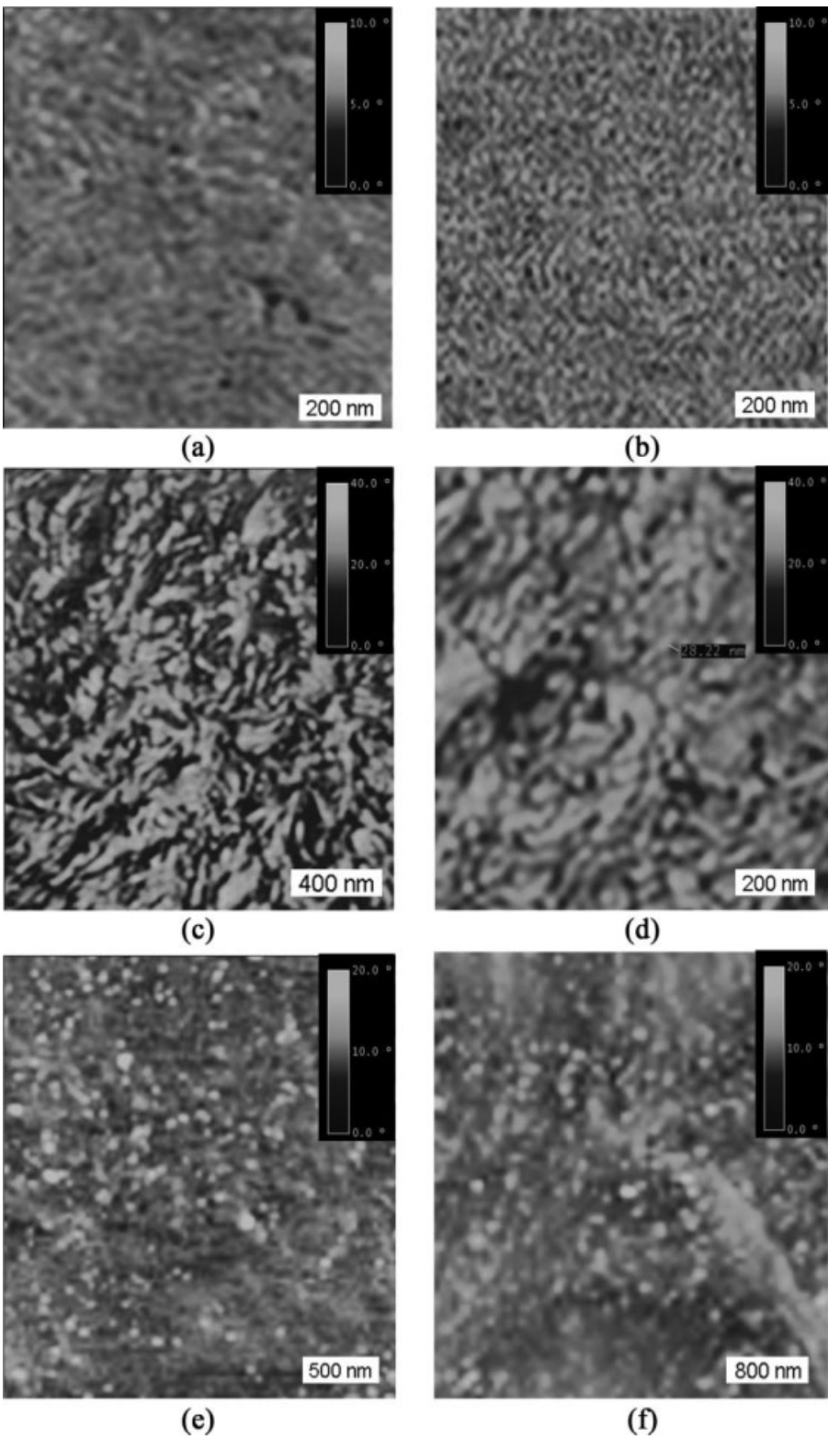

Figure 7 AFM phase images of thin films of PDMS-*s*-PBA and PDMS-*s*-PBCH copolymers with 25% (a and b), 40% (c and d), and 60% (e and f) PDMS content, respectively.

[Fig. 9(e,f)], the PDMS phase forms the dominant phase and the polyester segments segregate to form spheres. As expected, the size of these spheres varies, as a result of the copolymer synthesis method, where the polyester segments have various lengths and are randomly distributed in the copolymers. DSC results showed that the 60% PDMS content copolymers had very low percentage

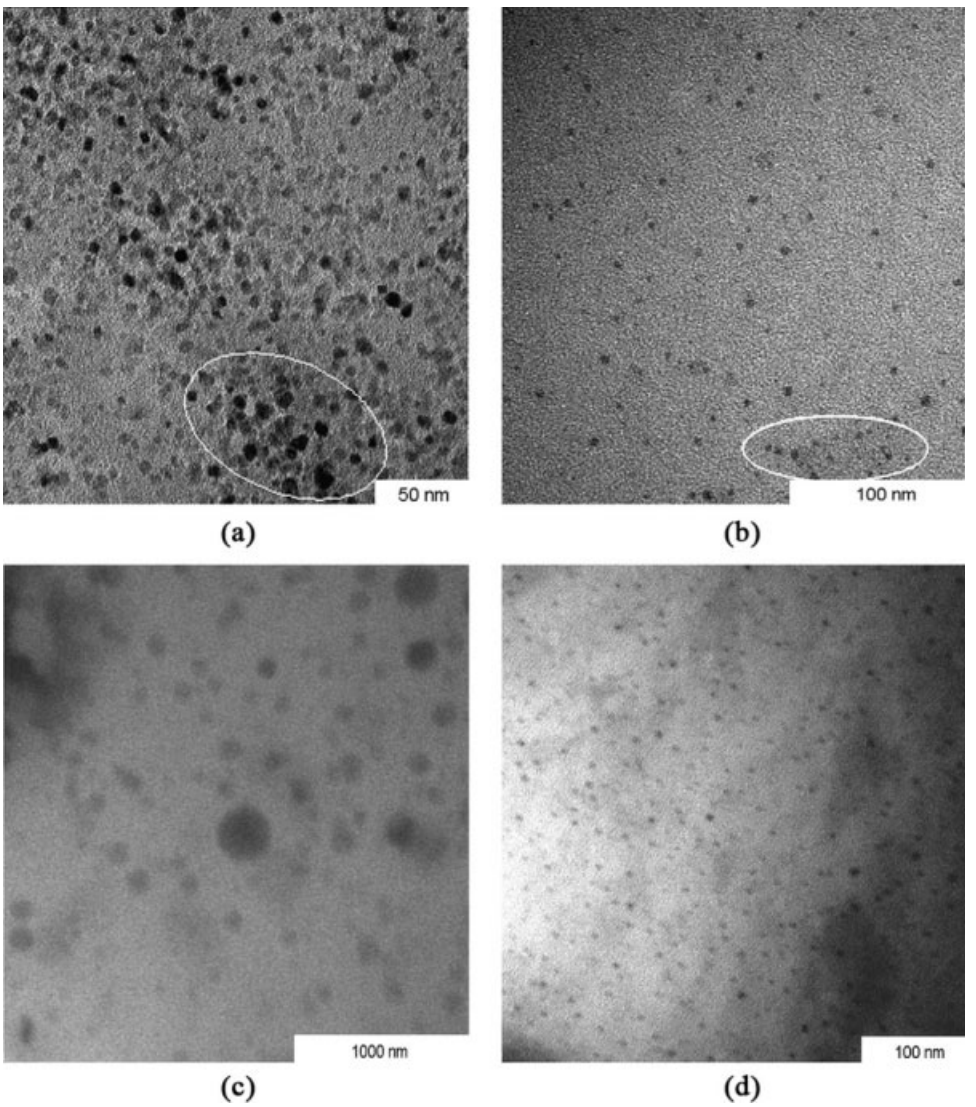

Figure 8 TEM micrographs of poly(dimethylsiloxane)–polyester copolymers: (a and c) PDMS-*s*-PBCH 5% and 10% PDMS content, respectively, and (b and d) PDMS-*s*-PBA 5% and 10% PDMS content, respectively.

crystallinity, and this is confined within the spherical domains.

CONCLUSIONS

Two series of hybrid PDMS-*s*-PBA and PDMS-*s*-PBCH copolymers were successfully synthesized via transesterification polymerization under vacuum conditions. The percentage of unreacted PDMS increased with an increase in the PDMS feed content for both types of polyester. The PDMS-*s*-PBA series had a higher quantity of unreacted PDMS than the PDMS-*s*-PBCH series. Both copolymer series did, however, show good PDMS incorporation with a higher PDMS feed ratio. A significant reduction in crystallinity of the copolymers in both copolymer series was observed as the PDMS content increased, as determined by WAXD and DSC. Moreover, the effect of the PDMS on the crystallinity degree was greater in the PDMS-*s*-PBCH copolymers series than in the PDMS-*s*-PBA copolymers series. This was attributed to either the higher chain mobility of the PBA segment when compared with the PBCH segment or the large difference in the polarity between the PDMS segment and the PBA segment when compared with the PBCH segment, which led to a higher degree of mixing in the PDMS-*s*-PBCH copolymer series than that in the PDMS-*s*-PBA copolymer series.

An investigation of the microscopic surface morphology of the copolymers, using AFM, showed that the PBA and PBCH homopolymers exhibited spherulite morphology. Both the PDMS-*s*-PBA and PDMS-*s*-PBCH copolymers with a 5% PDMS content showed spherulite morphology despite the ability of PDMS segments to segregate at the surface. The PDMS domains were observed between the lamella crystal structures on the surface of these copolymers.

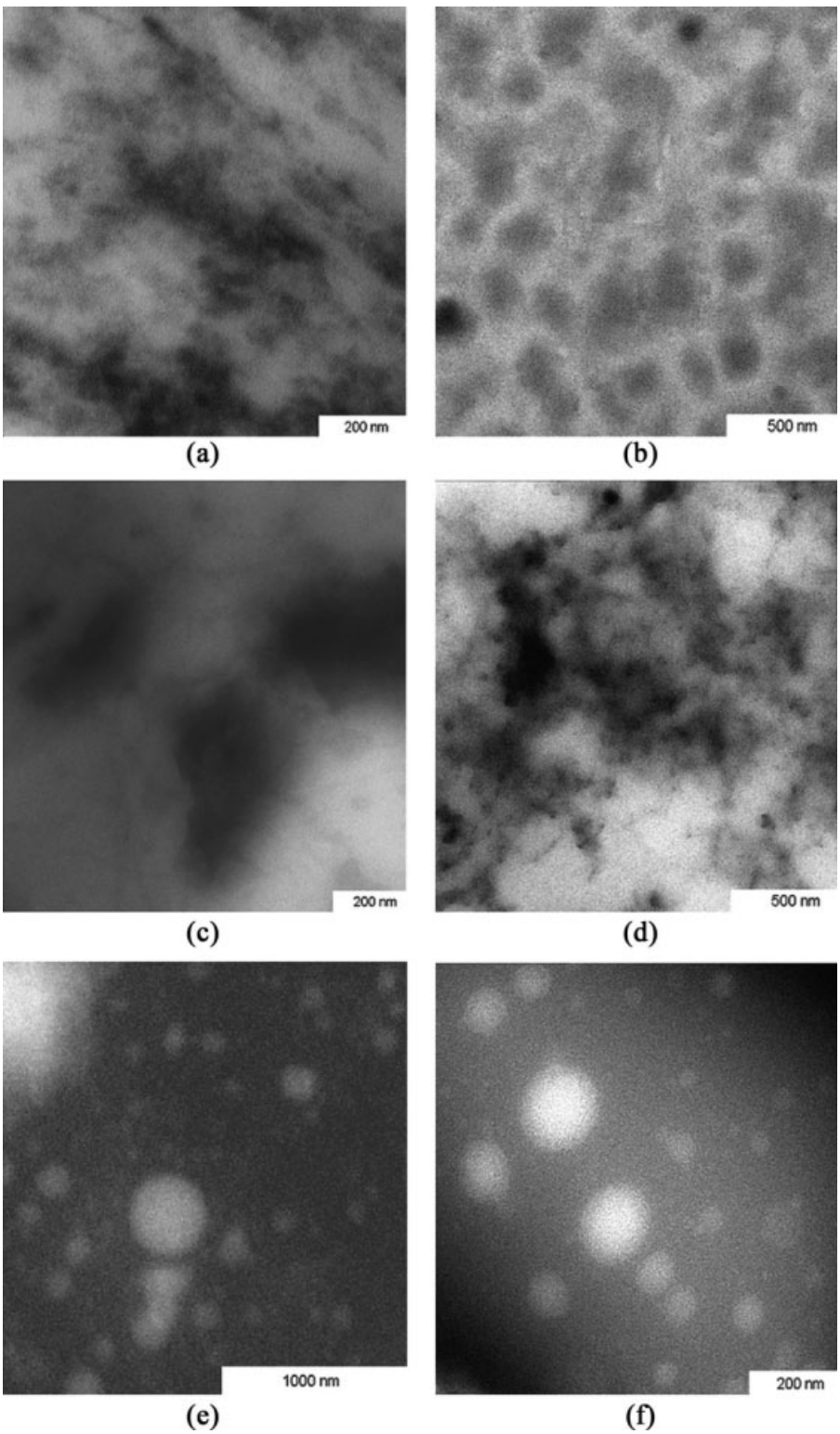

Figure 9 TEM micrographs of poly(dimethylsiloxane)–polyester copolymers: (a, c, and e) PDMS-*s*-PBCH 25, 40, and 60% PDMS content, respectively, and (b, d, and f) PDMS-*s*-PBA 25, 40, and 60% PDMS content, respectively.

This leads to a heterogeneous distribution of the PDMS domain within the polyester matrix. As the content of PDMS increased to 10%, the PDMS nanodomain distribution became more homogeneous for both copolymer series. In the case of the PDMS-*s*-PBA copolymer, however, the PDMS domains were clearly observed around the boundaries of the spherulites. The PDMS-*s*-PBCH copolymers showed clear microphase separation, in which the PDMS formed spherical domains in a matrix of PBCH and, in

contrast to PDMS-*s*-PBA, no spherulitic crystal structure was observed for PDMS-*s*-PBCH copolymers in AFM images. In the PDMS-*s*-PBA and PDMS-*s*-PBCH copolymers with 10% PDMS content, the diameters of the PDMS spheres were larger than the diameters measured for PDMS-*s*-PBA and PDMS-*s*-PBCH copolymers with 5% PDMS content. This was attributed to the increase in PDMS content and consequent increase in the PDMS segment lengths.

AFM images also showed that in both types of polyester copolymers, the copolymer surface morphology or the type of microphase separation is dependent on the PDMS content. When the PDMS content increased to 40%, the PDMS spheres completely disappeared and the morphology changed to a bicontinuous or co-continuous morphology. As the PDMS content increased above 50%, the PDMS phase formed the dominant phase and the polyester segments segregated to form spheres. The phase separation in segmented copolymers with random polyester segment length, and for low PDMS content, probably occurs by liquid–liquid demixing in combination with crystallization. The PDMS segments were able to segregate in between the lamella structure without destroying the spherulitic structure. This occurs only in the case of the low-content PDMS copolymers. On the other hand, the high PDMS contents copolymers show that crystallization was confined mainly within spherical, nanoscale domains in the bulk of the sample.

Furthermore, TEM results confirmed the multiphase bulk morphology that was detected by DMA and AFM for both copolymer series. Three types of morphologies were observed. Copolymers with a 5% PDMS content showed heterogeneously distributed spherical microdomains of PDMS in a matrix of polyester. As the content of the PDMS increased to 10%, the PDMS domain distribution became more homogeneous. At a PDMS content of 40%, a bicontinuous double-diamond type of morphology was observed in the TEM images, and when the PDMS content increased to 60%, spherical microdomains of polyester in a matrix of PDMS was observed for both copolymers.

The authors thank Remy Bucher from iThemba LABS, South Africa, for WAXD analysis, and Mohamed Jaffer from the University of Cape Town, South Africa, for TEM analysis. This work was partially funded by Center for Macromolecular Chemistry and Technology in Tripoli, Libya.

References

1. Yamamoto, N.; Mori, H.; Nakata, A.; Suehiro, M. U.S. Pat. 4,894,427 (1990).
2. Kiefer, L. A.; Yoon, T. H.; Glass, T. E.; Jayaraman, S. K.; McGrath, J. E. J Polym Sci Part A: Polym Chem 1997, 35, 3495.
3. Miroslawa, E. F. Des Monomers Polym 2000, 3, 325.
4. Vesna, V. A.; Milica, R. B.; Jasna, D. Polym Int 2001, 50, 1201.
5. Dojcinovic, B. P.; Vesna, V. A.; Vuckovic, M. V.; Jasna, D. J Serb Chem Soc 2005, 70, 1469.
6. Vuckovic, M. V.; Vesna, V. A.; Dojcinovic, B. P.; Govedarica, M. N.; Jasna, D. Polym Int 2006, 55, 1304.
7. Yilgör, I.; McGrath, J. E. Adv Polym Sci 1988, 86, 1.
8. Ekin, A.; Webster, D. C. J Polym Sci Part A: Polym Chem 2006, 44, 4880.
9. Rangarajan, P.; Register, R. A.; Adamson, D. H.; Fetters, L. J.; Bras, W.; Naylor, S.; Ryan, A. J. Macromolecules 1995, 28, 1422.
10. Ryan, A. J.; Hamley, W.; Bras, W.; Bates, F. S. Macromolecules 1995, 28, 3860.
11. Loo, Y.-L.; Register, R. A.; Ryan, A. J. Macromolecules 2002, 35, 2365.
12. Muller, A. J.; Balsamo, V.; Arnal, M. L. Adv Polym Sci 2005, 190, 1.
13. Fajun, Z.; Yongzhong, C.; Haiying, H.; Zhijun, H.; Tianbai, H. Langmuir 2003, 19, 5563.
14. Douzinas, K. C.; Cohen, R. E.; Halasa, A. F. Macromolecules 1991, 24, 4457.
15. Hamley, I. W.; Fairclough, J. P. A.; Terrill, N. J.; Ryan, A. J.; Lipic, P. M.; Bates, F. S.; Towns-Andrews, E. Macromolecules 1996, 29, 8835.
16. Stanciu, A.; Airinei, A.; Timpu, D.; Ioanid, A.; Ioan, C.; Bulacovschi, V. Eur Polym J 1999, 35, 1959.
17. Higuchi, A.; Nakagawa, T. J Polym Sci Part B: Polym Phys 1994, 32, 149.
18. Childs, M. A.; Matlock, D. D.; Dorgan, J. R.; Ohno, T. R. Biomacromolecules 2001, 2, 526.
19. Dong, T.; Kai, W.; Inoue, Y. Macromolecules 2007, 40, 8285.
20. Frömsdorf, A.; Woo, E. M.; Lee, L. T.; Chen, Y.-F.; Förster, S. Macromol Rapid Commun 2008, 29, 1322.
21. McGrath, J. E.; Dunson, D. L.; Mecham, S. J.; Hedrick James, L. Adv Polym Sci 1999, 140, 61.
22. Auman, B. C.; Percec, V.; Schneider, H. A.; Cantow, H.-J. Polymer 1987, 28, 1407.
23. Chang, S.-J.; Tsai, H.-B. J Appl Polym Sci 1994, 51, 999.
24. Hernandez, R.; Weksler, J.; Padsalgikar, A.; Runt, J. Macromolecules 2007, 40, 5441.
25. Small, P. A. J Appl Chem 1953, 3, 71.
26. Leclère, Ph.; Hennebicq, E.; Calderone, A.; Brocorens, P.; Grimsdale, A. C.; Müllen, K.; Brédas, J. L.; Lazzaroni, R. Prog Polym Sci 2003, 28, 55.
27. Daniels, R.; Magonov, S. U.S. Pat. 6,185,992, (2001).
28. Villers, D.; Dosière, M.; Paternostre, L. Polymer 1994, 35, 1586.
29. Magonov, S. N.; Elings, V.; Whangbo, M.-H. Surf Sci 1997, 375, L385.
30. Magonov, S. N.; Elings, V.; Papkov, V. S. Polymer 1997, 38, 297.
31. Bar, G.; Thomann, Y.; Brandsch, R.; Cantow, H. J.; Whangbo, M.-H. Langmuir 1997, 13, 3807.
32. Kowalewski, T.; McCullough, R. D.; Matyjaszewski, K. Eur Phys J E 2003, 10, 5.
33. Tamayo, J.; García, R. Appl Phys Lett 1997, 71, 2394.
34. Tamayo, J.; García, R. Appl Phys Lett 1998, 73, 2926.
35. Whangbo, M.-H.; Bar, G.; Brandsch, R. Surf Sci 1998, 411, L794.
36. Loo, Y.-L.; Register, R. A.; Ryan, A. J. Phys Rev Lett 2000, 84, 4120.
37. Van der Schuur, M.; Van der Heide, E.; Feijen, J.; Gaymans, R. J. Polymer 2005, 46, 3616.
38. Samorí, P.; Francke, V.; Mangel, T.; Müllen, K.; Rabe, J. P. Opt Mater 1998, 9, 390.
39. Rivetti, C.; Guthold, M.; Bustamante, C. J Mol Biol 1996, 264, 919.
40. Mahoney, C. M.; Gardella, J. A.; Rosenfeld, J. C. Macromolecules 2002, 35, 5256.
41. Chen, X.; Gardella, J. A., Jr.; Kumler, L. P. Macromolecules 1992, 25, 6631.
42. Liu, Y.; Zhao, W.; Zheng, X.; King, A.; Singh, A.; Rafailovich, M. H.; Sokolov, J.; Dai, K. H.; Kramer, E. J.; Schwarz, S. A.; Gebizlioglu, O.; Sinha, S. K. Macromolecules 1994, 27, 4000.
43. Ho, T.; Wynne, K. J.; Nissan, R. A. Macromolecules 1993, 26, 7029.